Automated Reference Points Selection for InSAR Time Series Analysis on Segmented Wetlands

Boya Zhang, Erin Hestir, Zhang Yunjun, *Member, IEEE*, Matthew E. Reiter, Joshua H. Viers, Danica Schaffer-Smith, Kristin Sesser, and Talib Oliver-Cabrera

***Abstract*— Interferometric synthetic aperture radar (InSAR) time series analysis is a powerful technique to estimate long-term water-level changes in wetland ecosystems. However, few studies have applied InSAR on wetlands that are highly segmented by canals and levees due in part to the challenge of selecting qualified reference points to minimize unwrapping errors, which, by contrast, is a relatively easy task for unsegmented wetlands. Here, we developed a new method to automatically select the optimal reference point for InSAR time series analysis. The method selects reference points by considering temporal behaviors of coherence and InSAR phase connectivity from each reference point to its wetland of interest. We tested the method on six managed and highly segmented wetland units within the Sacramento National Wildlife Refuge in the Central Valley, California. We validated the InSAR measurement against water depth gauge measurements during a low water depth (<10 cm) period in 2017. The overall accuracy of the estimated water depth changes achieved an RMSE of 1.49 cm. Compared with three existing methods, our method showed significantly lower RMSE values overall. This new automatic method enables us to maximize the performance of InSAR to predict water depth and could be applied to other types of InSAR applications as well.**

***Index Terms*— Coherence, connected component, reference point, water depths, wetland interferometric synthetic aperture radar (InSAR).**

I. Introduction

INTERFEROMETRIC synthetic aperture radar (InSAR) has been successfully applied to estimate water-level variations in both managed and natural wetlands [1], [2], [3], [4], [5], [6]. This application of remote sensing technology is most effective in wetlands with emergent herbaceous and woody vegetation with vertical structures above water surfaces, which enables double-bounce scattering [1], [2], [3]. Early studies used phase differences measured by a pair of SAR observations to estimate water-level change between two snapshots in time [1], [2], [3]. To satisfy the need of wetland management for continuous monitoring of water levels, recent studies used advanced time series analysis, such as small baseline subsets (SBASs), to estimate water-level variation across an extended time window (e.g., years) [5]. One of the critical steps for those InSAR applications is to select reference points with high and stable coherence over time and close to the target area, such as nearby residential areas [2]. Previous studies used a single reference point for wetlands of interest because they only focused on natural wetlands or managed wetland units with limited spatial segmentation [1], [2], [3] and thus only needed one stable point outside the wetland area.

However, the single reference point method may fail for highly segmented wetlands with distinct hydrologic regimes because of: 1) unwrapping errors among different wetland units and 2) decorrelation areas of vegetation that obstruct a coherent path from the reference location to the wetland of interest [6]. Large magnitude of rise and fall of water depths also causes unwrapping errors as an intrinsic InSAR limitation regardless of reference point selection. While multisegment processing (each segment with its own local reference point) recently proposed by Kang et al. [7] could mitigate the impact of decorrelation, it still requires manual reference point selection, which can be tedious and challenging even for experts. In addition, Cao et al. [8] and Zebker [9] proposed using average phase for multiple high-coherence pixels located outside of area of interest.

Our study developed an automatic reference point selection method for multitemporal InSAR applications. The method considers the location, coherence, and phase connectivity between the reference and wetland unit to maximize the phase connectivity between the two, thus minimizing the impact of unwrapping errors. We tested the method using highly segmented managed wetlands with areas much smaller than those of previous studies [1], [2], [3], [4], [5], [6]. The method builds upon the connected components from the phase unwrapping process and can be incorporated into open-source InSAR time series analysis packages, such as MintPy [10]. We tested the method using a C-band Sentinel-1 InSAR dataset over six segmented wetland units, where water depth gauge data were available, located within the Sacramento National Wildlife Refuge (Sacramento Refuge) in the Central Valley of California, USA [Fig. 1(a)]. This method can select an optimal reference for each unit. We compared water depth estimates

Manuscript received 3 December 2023; revised 26 February 2024 and 8 April 2024; accepted 10 April 2024. Date of publication 17 April 2024; date of current version 29 April 2024. This work was supported by the National Aeronautics and Space Administration (NASA) under Grant 80NSSC22K0935. *(Corresponding author: Boya Zhang.)*

Boya Zhang, Erin Hestir, and Joshua H. Viers are with the School of Engineering, University of California at Merced, Merced, CA 95343 USA (e-mail: bzhang64@ucmerced.edu).

Zhang Yunjun is with the Seismological Laboratory, California Institute of Technology, Pasadena, CA 91125 USA.

Matthew E. Reiter and Kristin Sesser are with the Point Blue Conservation Science, Petaluma, CA 94954 USA.

Danica Schaffer-Smith is with the Nature Conservancy, Durham, NC 27701 USA.

Talib Oliver-Cabrera is with the Jet Propulsion Laboratory, California Institute of Technology, Pasadena, CA 91109 USA.

This article has supplementary downloadable material available at https://doi.org/10.1109/LGRS.2024.3390568, provided by the authors.

Digital Object Identifier 10.1109/LGRS.2024.3390568

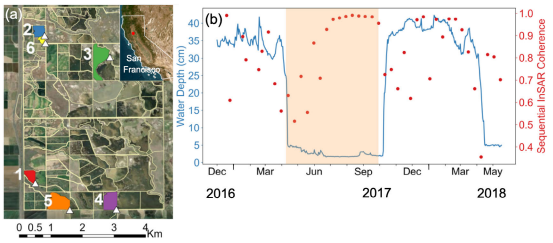

Fig. 1. (a) Location of the Sacramento Refuge with unit boundaries (yellow), six units, and water gauges (white triangles). (b) Time series of daily mean water depth of Unit 2 (left axis, blue line) and sequential InSAR coherence (between current and following adjacent date, right axis, red dot). Shaded areas represent InSAR processing time period.

from this automated reference point selection to water depth estimates using three existing reference selection methods. Since most wetlands in California are managed with limited information on water depth, which often differs among units, this study meets the urgent need to assist wetland resource managers in monitoring surface water depth.

II. Study Areas and Datasets

Managed wetlands in California provide important services, such as supporting millions of shorebirds and waterfowl [11], [12]. The Sacramento Refuge, primarily made up of emergent nontidal wetlands, is located in the northern Central Valley. The wetland hydrology is characterized by a seasonal pattern [Fig. 1(b)] of flooding and drawdowns. The wetland units are intentionally flooded from fall through spring, i.e., the wet season, from October to March [11]. The source of the flooding is subject to local rainfall and water allocation decisions by refuge managers. The Sacramento Refuge wetlands are highly segmented with a total number of 196 units across 4000 ha, with an average of ∼20 ha per unit [Fig. 1(a)]. We tested the reference point selection method using six wetland units [Fig. 1(a)], each outfitted with a pressure transducer water-level gauge measuring subdaily water depth from December 2016 to May 2018 (as shown in Fig. S1 for all six units). We obtained 10-m digital terrain models (DTMs) for each unit generated by the previous study via Real-Time Kinematic Survey [11].

This study used 43 C-band Sentinel-1A/B interferometric wide mode single look complex (SLC) from descending path 114 acquired during December 24, 2016 to May 13, 2018, which overlapped with measurements of water depths [Fig. 1(b)]. We used VV for analysis, which showed better performance in interferometry than VH [3].

We processed the set of coregistered and unwrapped interferograms, including unwrapped phase, coherence, and connected components, by employing the ISCE-2 topsStack processor and SNAPHU [13], [14], [15]. We connected each SAR acquisition with its nearest two neighbors in time to form interferograms. For each interferogram, we applied a Goldstein filter with a strength of 0.8, and a multilooking with a factor of two and six in azimuth and range directions, respectively, then geocoded into the WGS84 coordinate system at a ∼30-m grid. We used only the dry season when water depths were lower than 10 cm because high water depths and high variations lead to greater unwrapping error, which makes it difficult to test the

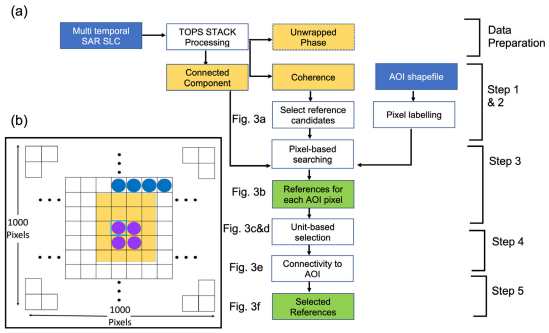

Fig. 2. (a) Flowchart of the five-step procedure. (b) Schematic plot for Step 3. The search grid is centered at a pixel within the AOI (with a light green square). Orange grids represent the extent of an AOI; purple pixels are pixels within the AOI; blue pixels are outside of the AOI.

TABLE I
Initial Threshold Parameters Used in This Study

Parameters	Values	Parameters	Values
coh_thd	0.9	*quality_thd*	30
perc_thd	0.95	*min_area*	30
edge	1000	*px_per_comp*	5
conn_perc_thd	0.8	*path_thd*	0.9

method. The low water-depth period is from April to October and varies between units (Fig. S1). We derived the relative water depth time series from the set of interferograms [3] using the small baseline approach implemented in the MintPy software [10].

III. Methodology

Given an area of interest (AOI, in this case, a wetland unit), the method automatically selects the reference point as a part of the procedure in InSAR time series analysis. The main goal of the method is to find optimal reference points that satisfy three criteria: 1) located outside but close to a wetland unit; 2) have high coherence values over time; and 3) have a coherent path, i.e., spatially adjacent pixels with high coherence values, from the reference to the AOI.

Data preparation obtains several products from topsStack processing. The unwrapped phase [the yellow rectangle in the data preparation step of Fig. 2(a)] is not used in the reference selection method but is used in later steps of InSAR processing. The reference selection method also requires a user-supplied geographic delineation of an AOI [e.g., shapefile data, Fig. 2(a)] with the same coordinate system (WGS84) as InSAR data. This study used the shapefile of the Sacramento National Wildlife Refuge generated from external resources. The method can be described as a five-step procedure as follows, with initial values defined in Table I for the datasets used in this study.

Step 1 labels the pixels using the AOI shapefile. Pixels outside of the AOI are labeled as 0 and those within as 1. For this study, selecting a reference within the AOI would cancel

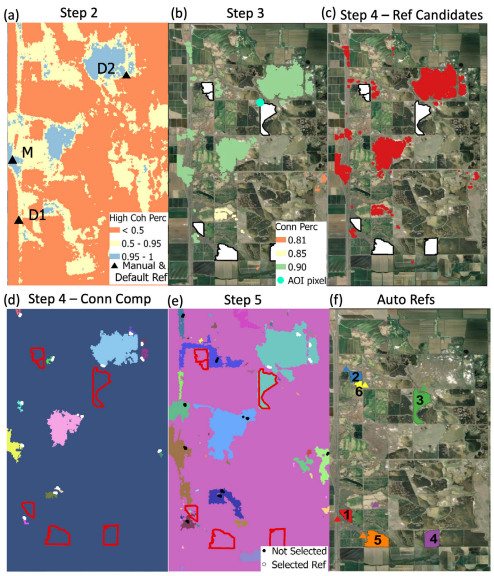

Fig. 3. Results for each step using Unit 3 as an example. (a) Percentage of high coherence in time and the locations of manually selected and MintPy default reference. (b) Percentage of connections to an AOI pixel (cyan dot). (c) and (d) Selected reference candidates and connected components in different locations. (e) Connected component based on mean coherence value (pink color is the background with a zero value) with selected and unselected reference points. (f) Locations of reference for each unit.

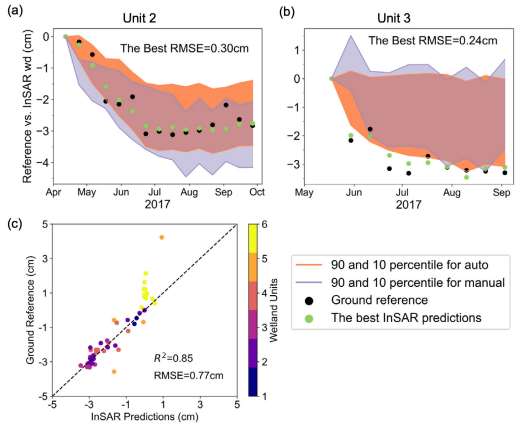

Fig. 4. (a) and (b) Example of the time series of InSAR and ground reference for Units 2 and 3, respectively. (c) Comparison between estimated water depths and ground reference using the pixel with the lowest RMSE from each unit.

out displacement signals due to homogeneous water-level changes in space.

Step 2 selects reference pixel candidates based on coherence values in time. This step identifies pixels with spatial coherence values greater than threshold *coh_thd* for more than *perc_thd* of InSAR pairs [blue patches, Fig. 3(a)].

Step 3 evaluates phase connectivity using a pixel-level iterative searching process for each pixel within an AOI. Based on the connected component, we calculate the percentage of InSAR pairs that the AOI pixel is connected to a reference candidate from Step 2. For each AOI pixel, this step searches for surrounding reference candidates within a square with a length of *edge* pixels [Fig. 3(b)]. For a reference candidate within the square [e.g., the cyan dot in Fig. 3(b)], if the percentage of connections to the AOI pixel is greater than a *conn_perc_thd* threshold, we identify it as a reference candidate [red, yellow, and green dots in Fig. 3(b)]. As a result, each AOI pixel has a list of reference candidates.

Step 4 selects reference points at the AOI level. To remove noisy AOI pixels (e.g., open water), we remove AOI pixels with less than *quality_thd* reference candidates. We intersect the reference candidate lists for all remaining AOI pixels to obtain a list of reference candidates that have high connections with all qualified AOI pixels [Fig. 3(c)]. If this step does not find any reference points, we decrease the *perc_thd* and *conn_perc_thd* parameters with an increment of 0.05. Since coherence is the priority for reference selection, parameter tuning prioritizes decreasing *conn_perc_thd*.

Step 4 conducts a connected component analysis to represent different locations of clusters of the reference candidates [Fig. 3(d)]. A *min_area* threshold is applied to remove clusters with a low number of candidates. For each component, we selected the top *px_per_comp* candidates with the shortest distance to the AOI [white dots, Fig. 3(d)].

Step 5 considers a coherent path between the reference candidates to the AOI. First, we generate a mask image based on a mean coherence image of all InSAR pairs using a threshold *path_thd*. The mask consists of 1 and 0 values, representing mean coherence greater or smaller than *path_thd*, respectively. We mark all the AOI pixels as 1 before conducting a connected component analysis for the mask image. For the reference obtained from Step 4 sharing the same connected component with the AOI pixels [Unit 3 and nearby component in Fig. 3(e)], meaning a coherent path exists between the candidate to the AOI, we select those as final reference points and rank them by the Euclidean distance to the AOI (the top one has the shortest distance). If the AOI is not connected to any component, we conduct an incremental dilation (step of 1) to surrounding pixels until the AOI is connected to a component.

IV. Results

We applied the method to each of the six wetland units in Sacramento Refuge and calculated water depth variation based on the selected reference points. Results from the method showed (1) the predicted water depth from InSAR compared to the ground reference (Fig. 4) and (2) the comparison between our automated method and other reference points (manually or algorithmically selected) in terms of accuracy for the estimated water depths (Figs. 4–6).

The hydrograph of Unit 2 in the Sacramento Refuge showed a clear seasonal pattern with low water depths from April to October when wetlands were drawn down [Fig. 1(b)]. Coherence data also showed a seasonal pattern with low and varying values in winter and spring when water depths were high, whereas coherence was relatively high and stable when water depth was low [shaded area in Fig. 1(b)], which was consistent with a previous study [16].

A. Reference Pixel Locations

By applying our automated method, we successfully found a reference point for each of the six units [Fig. 3(f)]. The

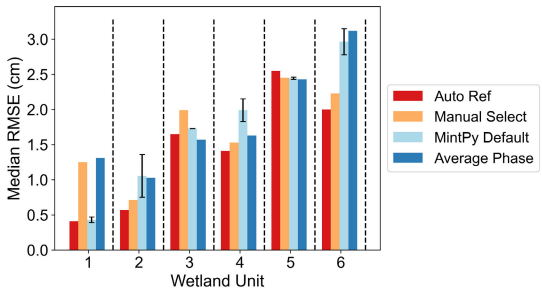

Fig. 5. Comparison of spatial median RMSE for six units among automatic and four other reference points. For MintPy default results, the color bar shows the average and error bar shows the RMSEs from the two default references.

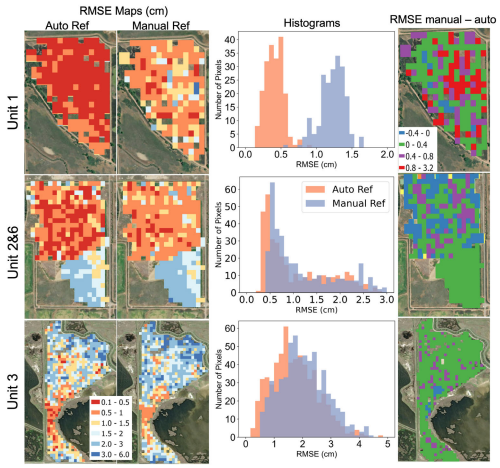

Fig. 6. Comparison of RMSE spatial distribution using the automatic and manual reference.

reference points were located close to the corresponding unit, had high coherence values in time, and high phase connectivity with a coherent path to the unit. We obtained multiple reference points for each unit and only showed the one closest to the AOI.

The default threshold parameters worked for most of the units with some exceptions. We tuned *conn_perc_thd* from 0.8 to 0.75 for Units 4 and 5 and additional tuning of *perc_thd* from 0.95 to 0.9 for Unit 4 to find a reference point. We also applied a dilation of 2 pixels for Units 1 and 3 in Step 5 to connect the unit to a close component [e.g., Unit 3 and a nearby component in Fig. 3(e)].

B. Validation of InSAR Estimated Water Depth

When estimating the time series of water depth, we set the starting date as the reference date for both InSAR and gauge water depth measurements [value of 0 for Fig. 4(a) and (b)]. Considering a gauge is located at marginal places for each unit [Fig. 1(a)] with relatively high terrain elevation, we only used wetland pixels with lower elevation values of the DTM than the gauge's elevation and, therefore, the pixel locations were consistently flooded. The water depth change from those wetland pixels was assumed to be the same as the changes in the gauge measurements considering a homogenous water surface for a unit. We showed the 90 and 10 percentiles of unit-wide InSAR results (using our automatic method and manual pixel) for each SAR date [Fig. 4(a) and (b)] and selected the pixel with the lowest RMSE for each unit [Fig. 4(c)]. Manual selected reference has higher RMSE, which is shown in Figs. 5 and 6. The pixels with the lowest RMSEs from each unit showed consistent InSAR results and ground reference with an R^2 of 0.85 and RMSE of 0.77 cm [Fig. 4(c)] and time series results showed that InSAR successfully tracked draw-down of the flooding [Fig. 4(a) and (b)]. Considering those results can be not representative of InSAR predictions over other pixels in space [e.g., Fig. 4(b)], we calculated, for each wetland unit, the spatial median of predictions for each time point (Fig. S2), which results in an overall RMSE of 1.49 cm using the automatic method and 1.69 cm for the manually selected reference point (results for each unit are shown in Figs. S2 and S3).

C. Comparison With the Existing Reference Selection Method

We compared the accuracy of predicted water depths for all six units among the automatic method (one reference for each unit) and the other four references, including a manually selected reference point, two points selected by the MintPy default setting, and average phase method proposed by [8], [9] with each reference used for six units (Fig. 5). The manually selected point is in the western part of the study area and it was characterized by (1) concrete road with high coherence (95% of InSAR pairs with a coherence value greater than 0.90) and (2) high-coherence pixels on the paths to all units [Fig. 3(a)]. The MintPy default references were selected based on (1) minimum average coherence of 0.85 and (2) located in the common connected component for all InSAR pairs. The last reference used the average unwrapped phase of all pixels outside the AOIs with coherence over 95% of time greater than 0.90 [e.g., blue areas in Fig. 3(a) for Unit 3].

We compared the spatial median RMSE among the five references for each unit (Fig. 5). The automatic reference points show, in general, lower RMSE than any other reference points. The only exceptions were (1) Unit 5 and (2) the average phase slightly outperformed ours for Unit 3. We also compared the spatial RMSE distributions between our reference and the manual selected point. For the manual point, the spatial distribution of RMSE of Units 1, 2, 6 (combined), and 3 clearly showed the advantage of using the algorithmically selected reference point compared to the manually selected point with lower RMSE values (Fig. 6). We used the Wilcoxon rank-sum statistical test to evaluate the difference among RMSE distributions resulting from the two methods and found that they were significantly different (Fig. 6, p-value < 0.05). We displayed the spatial distribution of temporal coherence and water depths change velocity in Figs. S4 and S5 and explained the reason of some high RMSE pixels in Unit 3 in Fig. S6. Overall, the automatic approach outperformed the manual selection for five out of six units, and only Unit 5 showed a higher RMSE.

V. Discussion and Conclusion

Our study developed a method for automatically selecting optimal reference points for multitemporal InSAR SBASs analysis. We showed the effectiveness of the method by estimating long-term water depth variations in small, hydrologically distinct managed wetlands in the Sacramento Refuge,

TABLE II
SUMMARY OF INSAR PERFORMANCE IN WETLAND UNITS

Unit	Auto better ?	InSAR consistent with ref?	Comment
1-4, 6	Yes	Yes	High RMSE in part of Unit 3&4 due to low vegetation density (Fig.S6)
5	No	No	Unwrap errors from water rise & fall

California. The method evaluates coherence behavior and connectivity between a reference candidate to the AOI (wetland unit in this case). We tested the method on six wetland units, a highly segmented landscape challenging for InSAR. The method successfully found optimal reference points for each unit, which were used to generate accurate estimates of water depth changes.

When compared to the other references, the automatic unit-based references achieved better results in most of the cases with a few exceptions in Units 3 and 5. Our method outperforms the average phase method for five of the six units except Unit 3 with slightly lower accuracy (Fig. 5). Errors for Unit 5 are mostly contributed by unwrapping errors due to large water depth variations instead of reference points (Fig. S2 for details). The selected reference can correct errors due to incoherent barriers between reference point and AOI but not the errors due to large spatial phase gradients. The automatic method does not necessarily result in better accuracy, but it achieves comparable accuracy to a manually or algorithmically selected point. We summarized the InSAR performance over six units in Table II.

One advantage of our method is to consider the coherent path between the reference point to the AOI. For example, our method outperformed the manually selected point for Unit 3 because there is no coherent path between the point and the unit [Fig. 3(e)], which introduced unwrapping errors that resulted in lower accuracy for the predicted water depths. Note that the manually selected point showed high connectivity to the AOI unit [Fig. 3(c)] using the connected component generated by SNAPHU. We found that SNAPHU often showed that connected components included pixels with relatively low coherence values, which is partly due to the limit of the number of components. We successfully used a mask derived from the mean coherence to generate a new connected component that filters the reference candidates with coherent paths to the AOI to achieve better accuracy.

For future applications, users should adjust the parameters in Table I based on InSAR stack parameters and knowledge of local wetland environments. For example, *perc_thd* and *conn_perc_thd* should change with the number of connected neighbors. For computational performance, Step 3 is the most time-consuming part. However, this can be easily reduced in practice via (1) parallel processing and (2) sampling a subset of the pixels within the searching square.

This new InSAR-based reference selection method not only has great potential for understanding regional wetland hydrology for other managed wetlands located in California but also scientific value for other types of InSAR applications for the upcoming NASA-ISRO SAR (NISAR).

ACKNOWLEDGMENT

The Sentinel-1 data were provided by ESA from Alaska Satellite Facility. The research was carried out under a National Aeronautics and Space Administration project. This work was done as an outside activity and not in the capacity of Talib Oliver-Cabrera as an employee of the Jet Propulsion Laboratory, California Institute of Technology.

CODE AVAILABILITY

The algorithm is implemented in Python and available at https://github.com/geopaulzhang/auto-ref-point.git and https://doi.org/10.5281/zenodo.10866853.

REFERENCES

[1] B. Zhang, S. Wdowinski, T. Oliver-Cabrera, R. Koirala, M. J. Jo, and B. Osmanoglu, "Mapping the extent and magnitude of sever flooding induced by Hurricane Irma with multi-temporal Sentinel-1 SAR and InSAR observations," *Int. Arch. Photogramm., Remote Sens. Spatial Inf. Sci.*, vol. 3, pp. 2237–2244, Apr. 2018.

[2] Z. Chen et al., "Characterizing Marsh wetlands in the great lakes basin with C-band InSAR observations," *Remote Sens. Environ.*, vol. 242, Jun. 2020, Art. no. 111750.

[3] H. Liao, S. Wdowinski, and S. Li, "Regional-scale hydrological monitoring of wetlands with Sentinel-1 InSAR observations: Case study of the South Florida Everglades," *Remote Sens. Environ.*, vol. 251, Dec. 2020, Art. no. 112051.

[4] B. Zhang, S. Wdowinski, D. Gann, S.-H. Hong, and J. Sah, "Spatiotemporal variations of wetland backscatter: The role of water depth and vegetation characteristics in Sentinel-1 dual-polarization SAR observations," *Remote Sens. Environ.*, vol. 270, Mar. 2022, Art. no. 112864.

[5] S.-H. Hong, S. Wdowinski, S.-W. Kim, and J.-S. Won, "Multi-temporal monitoring of wetland water levels in the Florida Everglades using interferometric synthetic aperture radar (InSAR)," *Remote Sens. Environ.*, vol. 114, no. 11, pp. 2436–2447, Nov. 2010.

[6] T. Oliver-Cabrera, C. E. Jones, Z. Yunjun, and M. Simard, "InSAR phase unwrapping error correction for rapid repeat measurements of water level change in wetlands," *IEEE Trans. Geosci. Remote Sens.*, vol. 60, 2022, Art. no. 5215115.

[7] Y. Kang, Z. Lu, C. Zhao, Y. Xu, J.-W. Kim, and A. J. Gallegos, "InSAR monitoring of creeping landslides in mountainous regions: A case study in Eldorado National Forest, California," *Remote Sens. Environ.*, vol. 258, Jun. 2021, Art. no. 112400.

[8] Y. Cao, Z. Li, and F. Amelung, "Mapping ground displacement by a multiple phase difference-based InSAR approach: With stochastic model estimation and turbulent troposphere mitigation," *J. Geodesy*, vol. 93, no. 9, pp. 1313–1333, Sep. 2019.

[9] H. Zebker, "Accuracy of a model-free algorithm for temporal InSAR tropospheric correction," *Remote Sens.*, vol. 13, no. 3, p. 409, Jan. 2021.

[10] Z. Yunjun, H. Fattahi, and F. Amelung, "Small baseline InSAR time series analysis: Unwrapping error correction and noise reduction," *Comput. Geosci.*, vol. 133, Dec. 2019, Art. no. 104331.

[11] D. Schaffer-Smith, J. J. Swenson, M. E. Reiter, and J. E. Isola, "Quantifying shorebird habitat in managed wetlands by modeling shallow water depth dynamics," *Ecol. Appl.*, vol. 28, no. 6, pp. 1534–1545, Sep. 2018.

[12] Central Valley Joint Venture (CVJV), *Central Valley Joint Venture 2020 Implementation Plan*. U.S. Fish and Wildlife Service, Sacramento, CA, USA, 2020.

[13] P. A. Rosen, E. Gurrola, G. F. Sacco, and H. Zebker, "The InSAR scientific computing environment," in *Proc. 9th Eur. Conf. Synth. Aperture Radar*, Apr. 2012, pp. 730–733.

[14] H. Fattahi, P. Agram, and M. Simons, "A network-based enhanced spectral diversity approach for Tops time-series analysis," *IEEE Trans. Geosci. Remote Sens.*, vol. 55, no. 2, pp. 777–786, Feb. 2017.

[15] C. W. Chen and H. A. Zebker, "Phase unwrapping for large SAR interferograms: Statistical segmentation and generalized network models," *IEEE Trans. Geosci. Remote Sens.*, vol. 40, no. 8, pp. 1709–1719, Aug. 2002.

[16] B. Zhang et al., "Multi-temporal analysis of InSAR coherence, NDVI, and in situ water depths for managed wetlands in national wildlife refuges, California," in *Proc. IEEE Int. Geosci. Remote Sens. Symp.*, Jul. 2023, pp. 8186–8189.